Materials Advances

ROYAL SOCIETY OF CHEMISTRY

PAPER

View Article Online
View Journal | View Issue

Cite this: *Mater. Adv.*, 2025, 6, 5269

Controlled release of aminomethylenebisphosphonates from a calcium zeolite carrier: investigating the impact of compound structure on sorption and release profiles†

Monika Zielińska, *[a] Natalia Banaś,[a] Rozalia Gałecka,[a] Ewa Chmielewska,[b] Maria Ratajczak,[c] Michael Fischer,[d] Paulina Lechwar,[e] Katarzyna Gaweł-Bęben,[e] Adam Voelkel[a] and Mariusz Sandomierski[a]

This study investigates the controlled release of the aminomethylenebisphosphonates from a calcium-exchanged zeolite carrier and explores the influence of compound structure on sorption and release profiles. Thirteen bisphosphonates (BPs), including risedronate (RSD), were tested for their sorption capacity and release behavior in simulated body fluid (SBF). Sorption studies revealed that BPs with iodine, methyl, and benziothiazole groups (BP5, BP6, and BP12) exhibited high sorption rates (>50%), while compounds containing bromine or chlorine displayed lower sorption capacities. Release experiments demonstrated that RSD, BP5, and BP6 followed a sustained release profile, while BP12 showed an initial burst followed by a tapering release. The density functional theory (DFT) calculations provided further insight into the adsorption mechanisms, highlighting the role of dispersion interactions and electrostatic bonding with calcium ions. The use of zeolite carriers reduced the toxicity of drugs towards human fibroblast BJ cells. The effect of the carrier addition on osteosarcoma 143b cells was also determined; some of the drugs did not lose their activity in relation to them after being placed on the carrier. These findings suggest that calcium-exchanged zeolite carriers can effectively facilitate the controlled release of BPs, offering potential for applications in osteoporosis treatment by maintaining therapeutic levels over extended periods.

Received 16th April 2025,
Accepted 20th June 2025

DOI: 10.1039/d5ma00371g

rsc.li/materials-advances

1. Introduction

Bisphosphonates (BPs), a class of drugs with a high affinity for hydroxyapatite, have been widely used in the treatment of various bone-related disorders. While they are primarily associated with osteoporosis management, their therapeutic potential extends beyond this condition. These compounds play a crucial role in managing skeletal complications in metastatic bone disease, multiple myeloma, and Paget's disease of bone.[1] Moreover, BPs have been explored for their potential in treating bone sarcomas, particularly osteosarcoma, where they exhibit anti-tumor effects by inhibiting osteoclast-mediated bone resorption and tumor-induced osteolysis.[2,3] Additionally, emerging evidence suggests their efficacy in conditions such as fibrous dysplasia and hypercalcemia of malignancy, broadening their scope of clinical application.[1,4]

Osteosarcoma is the most common primary malignant bone tumor, predominantly affecting adolescents and young adults. Standard treatment involves neoadjuvant chemotherapy, surgical resection, and adjuvant chemotherapy, yet survival rates remain low for patients with metastatic or recurrent disease.[1] Recent studies suggest that BPs, particularly nitrogen-containing derivatives like zoledronic acid and alendronate, may have therapeutic potential beyond bone resorption inhibition. These compounds exhibit anti-tumor activity through multiple mechanisms, including inhibition of

[a] Institute of Chemical Technology and Engineering, Poznań University of Technology, Poznań, Poland. E-mail: monika.zielinska@put.poznan.pl
[b] Department of Bioorganic Chemistry, Faculty of Chemistry, Wrocław University of Science and Technology, Wrocław, Poland
[c] Institute of Building Engineering, Poznan University of Technology, ul. Piotrowo 5, 60-965 Poznań, Poland
[d] Crystallography & Geomaterials Research, Faculty of Geosciences, and Bremen Center for Computational Materials Science, and MAPEX Center for Materials and Processes, University of Bremen, Bibliothekstraße 1, D-28359 Bremen, Germany
[e] Department of Cosmetology, University of Information Technology and Management in Rzeszów, Sucharskiego 2, 35-225 Rzeszów, Poland

† Electronic supplementary information (ESI) available. See DOI: https://doi.org/10.1039/d5ma00371g

osteoclast-mediated bone resorption, suppression of angiogenesis, and induction of apoptosis in osteosarcoma cells.[3] Moreover, BPs interfere with tumor-induced osteolysis by attenuating the expression of receptor activator of NF-κB ligand (RANKL) and monocyte chemoattractant protein-1 (MCP-1), key factors involved in the recruitment and activation of osteoclasts.[5] Despite promising preclinical results, clinical trials evaluating the addition of BPs to conventional chemotherapy regimens have yielded mixed results, highlighting the need for further investigation into their role as adjuvant therapies in osteosarcoma treatment.[2]

While BPs have been extensively studied in osteosarcoma and other malignancies, their most well-established application remains osteoporosis treatment. Osteoporosis, characterized by a decrease in bone mineral density and structural imbalances within bone tissue, increases the risk of fractures, particularly in vulnerable areas such as the vertebrae, hip, and wrist.[6,7] Treating and preventing osteoporosis, which affects millions of individuals in the European Union, involves lifestyle changes, proper nutrition, and, in some cases, medication to address this significant health concern, especially among older adults.[8]

The use of BPs, like alendronate and risedronate, as the preferred initial treatment for osteoporosis is due to their ability to inhibit osteoclast activity, maintaining bone density and reducing fracture risk. Beyond osteoporosis, these medications are also utilized in treating conditions like Paget's disease and preventing bone complications in specific cancers, typically taken orally or *via* intravenous administration.[9,10]

BPs have a high affinity for binding to hydroxyapatite (a component of bone) due to their structural properties, specifically the presence of phosphate groups that allow them to interact with the calcium ions in hydroxyapatite crystals.[11] This interaction leads to adsorption and eventual incorporation of BPs into the bone matrix, contributing to their effectiveness in treating these conditions. Recent research indicates that the effectiveness of BPs in mineral binding is influenced not just by the P–C–P structure but also by the R2 side chains, with nitrogen-containing BPs like alendronate and risedronate exhibiting notably higher potency compared to their counterparts without nitrogen.[12–14] The structural composition of BPs plays a crucial role in their interactions with hydroxyapatite, influencing factors such as uptake, retention by bones, internal diffusion, and release mechanisms of the drug, as revealed by established structure–activity relationships.[11,15]

The challenges associated with the oral administration of BPs, attributed to their low bioavailability and absorption limitations in the proximal duodenum, necessitate specific guidelines for optimal intake.[16] These guidelines recommend taking the medication at least 30 minutes before the first meal, avoiding concomitant ingestion with food or other medications rich in divalent cations, and maintaining an upright posture during and after ingestion to minimize gastrointestinal side effects.[17] The first adverse reaction that appears is gastrointestinal irritation, leading to symptoms such as heartburn, esophageal irritation, stomach pain, nausea, and difficulty swallowing.[13] Besides gastrointestinal issues, potential adverse reactions to BPs include bisphosphonate-related osteonecrosis of the jaw, characterized by non-healing exposed bone in the facial region, and an increased risk of atypical femur fractures with long-term use, reinforcing the importance of cautious administration and monitoring.[18–20]

Considering the challenges linked to BP oral intake, novel carriers and active substances are being sought that, when combined, could offer a competitive and more efficient approach in combating osteoporosis. Zeolites are versatile biocompatible materials known for their three-dimensional microporous structure, showcasing diverse biomedical applications such as biomolecule separation,[21] drug delivery,[22–24] wound dressing,[25] and biosensor construction.[26,27] In addition to their documented properties as drug carriers, zeolites have recently emerged as promising materials in bone tissue engineering. Their porous structure and cation-exchange capacity support osteoblast adhesion and growth, while their similarity to bone mineral makes them suitable for implant coatings and bone regeneration strategies.[28–30] Zeolites have been successfully investigated as scaffold materials due to their porous structure and ability to promote osteoblast adhesion, proliferation, and differentiation.[28,30] They also exhibit osteoconductive and osteoinductive properties, making them promising candidates for implant coatings.[28] Furthermore, *in vitro* studies have confirmed their ability to enhance the proliferation and mineralization of pre-osteoblastic MG-63 cells, underlining their relevance in bone tissue engineering.[29] This study centers on zeolite type X, characterized by sodalite cages, and a Si/Al ratio between 1 to 1.5, which exhibits underexplored potential as a drug carrier. Previous research utilized this zeolite for BP delivery by leveraging its calcium-exchanged form, demonstrating sustained drug release over 100 hours without a burst release effect.[31] Previous studies available in the literature have focused solely on commercial bisphosphonates (zoledronate and risedronate) and have not extensively addressed the impact of the molecular structure on their sorption onto the zeolite surface.[23,32] Moreover, these studies did not investigate the effect of zeolite X, either before or after drug loading, on cells, indicating that this research area has not yet been fully explored. Further exploration involving different API and carrier combinations is deemed crucial, as varying configurations can significantly influence drug release profiles and retention amounts, potentially broadening the scope of drug delivery applications in areas like intravenous delivery, scaffold delivery, and implant delivery using zeolite carriers. The compounds selected for this work, previously tested for their affinity to hydroxyapatite (the main bone-building material), showed that all twelve aminomethylenebisphosphonates had equal or stronger affinity for hydroxyapatite compared to the control compound RSD.[12,33]

The aim of this study is to investigate the controlled release properties of aminomethylenebisphosphonates from a calcium-exchanged zeolite carrier, providing insights into their potential for sustained therapeutic applications. Additionally, the study evaluates the sorption and release behavior of these BPs on the zeolite carrier. New calcium zeolite drug carriers with various BP drugs were extensively characterized and the

work attempted to determine the effect of drug structure on sorption both experimentally and computationally. Additionally, cell studies were conducted to determine the toxicity and the effect of the carrier on the retention of drug activity.

2. Materials and methods

2.1. Materials

Sodium risedronate (RSD), tris(hydroxymethyl)aminomethane (998%) (TRIS), and sodium zeolite 13X (Na-X, ~2 μm average particle size) were obtained from Sigma-Aldrich (Steinheim, Germany). Hydrochloric acid (36–38%), calcium chloride and sodium chloride (99%) were obtained from POCh (Gliwice, Poland). Each solution was prepared using ultrapure water (Arium® Pro Ultrapure Water System, Sartorius, Göttingen, Germany). Twelve aminomethylenebisphosphonates used in this study (Table 1) were prepared according to the procedure described previously.[12]

2.2. Ion exchange

Ion exchange was performed on Na-X zeolite (4 g) by mixing it with 70 ml of a 0.5 M solution of a calcium chloride for 24 hours, followed by centrifugation and repeated washing with distilled water. This procedure was repeated three times. The resulting material was then dried at 100 °C for 24 hours, mirroring the preparation process outlined in the previous publication.[23]

2.3. BP sorption

The zeolite samples (20 mg) were placed in polypropylene tubes and exposed to a solution of BPs (0.7 mM) in TRIS buffer. After a week, the sorption level was assessed, with additional weekly stages conducted if sorption exceeded 50%. Several BPs underwent three sorption cycles, involving shaking with a laboratory rotator mixer, centrifugation at 4000 rpm for 10 minutes, and analysis of sorption through UV spectroscopy on the centrifuged liquid.

2.4. BP release

The zeolites containing the sorbed BPs were immersed in 5 ml of simulated body fluid (SBF) with a pH of 7.4, prepared based on the method outlined by Kokubo *et al.*[39] SBF included in its composition (grams per 1000 ml of SBF): NaCl (8.035), $NaHCO_3$ (0.355), KCl (0.225), $K_2HPO_4{\cdot}3H_2O$ (0.231), Na_2SO_4 (0.072), TRIS (0.6112), and HCl. The amount of BPs released was measured after different time periods up to 198 h using UV-VIS spectroscopy. Before each measurement, the samples were centrifuged at 4000 rpm for 10 minutes followed by replenishing the SBF to ensure a fresh ion supply.

A new batch of SBF was prepared weekly to ensure its integrity and consistency throughout the experiment.[40]

To further investigate the mechanisms underlying the observed release behavior, the experimental data were fitted to three commonly used kinetic models: pseudo-first-order (one-phase decay), Higuchi, and Korsmeyer–Peppas. Nonlinear regression was performed using GraphPad Prism, and model fits were evaluated based on the coefficient of determination (R^2).

2.5. Scanning electron microscopy (SEM)/energy dispersive spectroscopy (EDS)

The scanning electron microscope VEGA3 (TESCAN, Czech Republic) was utilized to capture images of the obtained materials. This apparatus is also equipped with an energy dispersive X-ray spectroscopy (EDS) device (Bruker, UK). EDS was employed to analyze the elemental composition of the samples.

2.6. X-ray diffractometry (XRD)

The sample was examined by X-ray diffraction using a D8 Advance diffractometer (Bruker, UK) with a LynxEye detector. XRD measurements were performed using a non-monochromatic Cu-Kα beam in the Bragg–Brentano θ–2θ geometry with a Ni filter.

2.7. Elemental analysis

The measurements were conducted using a FLASH 2000 elemental analyzer. Samples, each weighing approximately 2 mg, were placed in tin capsules and introduced into the reactor *via* an autosampler, along with a precisely measured amount of oxygen. After being combusted at temperatures ranging from 900 to 1000 °C, the resulting flue gases were carried by a helium flow to the reactor's secondary furnace, which was filled with copper. The gases then passed through a water trap and into a chromatographic column, where they were separated into individual components. The separated gases were then detected using a thermal conductivity detector.

2.8. UV-VIS spectroscopy

The measurements were conducted in the range of 210–400 nm using a UV-VIS spectrophotometer (JASCO V-630, Japan) for the determination of the compound concentration during the sorption and release process. The quantitative assessment was performed based on the calibration curve method at the absorbance maximum for each BP (absorption properties of the tested compounds are summarized in Table 2).

2.9. Density functional theory calculations

To investigate the adsorption of BP drugs in calcium-exchanged zeolite X (CaX) on an atomistic level, density functional theory (DFT) calculations were carried out. The structure model of CaX used is the same as in our previous work (unit cell composition $Ca_{44}[Al_{88}Si_{104}O_{384}]$).[41] Out of all BPs, the species BP3, BP5, BP6, and BP7 were considered in the calculations. For each BP, a preliminary conformational screening was done using the conformers module of the DS BIOVIA Materials Studio suite, using the COMPASSIII force field.[42] Ten low-energy conformers were then optimized according to the DFT protocol outlined below. The lowest-energy conformer of each BP was inserted into the zeolite pores and different adsorption configurations were generated using a simulated annealing approach, which combined the Adsorption Locator and Forcite modules of Materials Studio and used, again, COMPASSIII parameters. From the collection of

Table 1 Structures of bisphosphonates (BPs) used in this study

No.	Compound name	Compound structure	Ref.
RSD	Risedronate	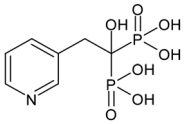	11
BP1	2-Pyridinylaminomethylene-1,1-bisphosphonic acid	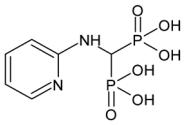	34
BP 2	(3-Methyl-2-pyridinyl)aminomethylene-1,1-bisphosphonic acid	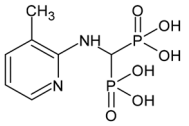	35
BP 3	(4-Methyl-2-pyridinyl)aminomethylene-1,1-bisphosphonic acid	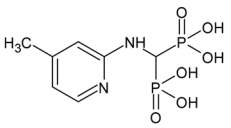	34
BP 4	(5-Methyl-2-pyridinyl)aminomethylene-1,1-bisphosphonic acid	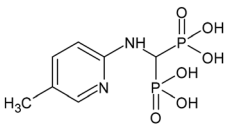	35
BP 5	(4,6-Dimethyl-2-pyridinyl)amino-methylene-1,1-bisphosphonic acid	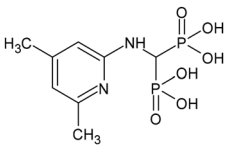	12 and 36
BP 6	(5-Iodo-2-pyridinyl)amino-methylene-1,1-bisphosphonic acid	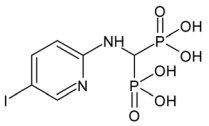	12 and 36
BP 7	(5-Bromo-2-pyridinyl)amino-methylene-1,1-bisphosphonic acid	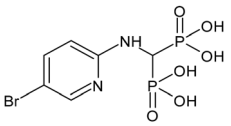	37
BP 8	(5-Chloro-2-pyridinyl)amino-methylene-1,1-bisphosphonic acid	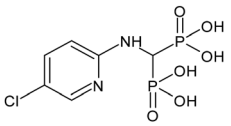	35
BP 9	(6-Chloro-2-pyridinyl)amino-methylene-1,1-bisphosphonic acid	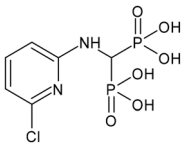	12
BP 10	(2-Chloro-3-pyridinyl)amino-methylene-1,1-bisphosphonic acid	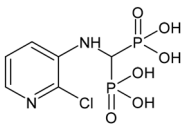	38
BP 11	(6-Hydroxy-2-pyridinyl)amino-methylene-1,1-bisphosphonic acid	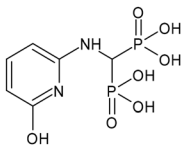	12

Table 1 (*continued*)

No.	Compound name	Compound structure	Ref.
BP 12	*N*-(1,3-Benzothiazol-2-yl)amino-methylene-1,1-bisphosphonic acid	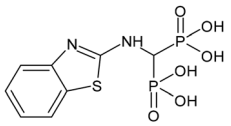	10

configurations generated in this way, eight low-energy configurations were extracted and optimized using DFT.

All DFT optimizations used the Quickstep code[43] that is integrated in the CP2K package[44] version 2024.1. The calculations used the dispersion-corrected B97-D3 functional.[45–47] In the Gaussian and plane wave (GPW) approach implemented in Quickstep, and "molecularly optimized" (MOLOPT)[48] basis sets of triple-zeta quality (TZVP-MOLOPT) were employed together with a planewave cutoff energy of 900 Ry for the finest integration grid. Goedeker–Teter–Hutter pseudopotentials devised by Krack were used to represent core electrons.[49] All atomic coordinates were fully optimized, fixing the cell parameter of CaX to the optimized value obtained for the guest-free system (cubic cell, a = 25.157 Å). After optimizing a given BP@CaX configuration, the adsorption energy was calculated by subtracting the DFT total energies of CaX and BP from the total energy of the combined system:

$$\Delta E_{\mathrm{ads}} = E_{\mathrm{DFT}}(\mathrm{BP@CaX}) - E_{\mathrm{DFT}}(\mathrm{CaX}) - E_{\mathrm{DFT}}(\mathrm{BP})$$

For each BP, the averaged adsorption energy $\Delta\bar{E}_{\mathrm{ads}}$ was calculated using a Boltzmann averaging (T = 298 K) over all eight configurations, as done in earlier work.[50] For the lowest-energy configurations, the relative contribution of dispersion interactions to the total adsorption energy was also calculated.

2.10. *In vitro* cytotoxicity studies

Human fibroblasts BJ (ATTC CRL-2522) and osteosarcoma 143b (ATCC CRL-8303) were purchased from LGC Standards (Łomianki, Poland) and maintained in Eagle's minimum essential medium (EMEM) or Dulbecco's modified Eagle's medium (DMEM), respectively, supplemented with 10% (v/v) foetal bovine serum (FBS) from Pan Biotech (Aidenbach, Germany). For each experiment 2×10^4 cells were plated onto 96-well plates and incubated overnight followed by 48 h or 72 h treatment with appropriate amounts of free BPs or BPs with zeolite carriers (final concentration of the BPs: 10–100 μM). Similar experiments were performed using RSD and RSD with zeolite carrier. The viability of the cells was then analysed using a neutral red uptake test,[51] as described previously. The cellular morphology was documented with an inverted microscope (Nikon Eclipse, Nikon, Tokyo, Japan) connected to a ProPad-5 camera (Euromex, Duiven, Netherlands).

2.11. Statistical analysis

Statistical analysis was carried out for all the obtained results. Sorption and BP release experiments were performed as five independent repetitions and three technical repetitions if necessary. A statistical significance of differences between the means of the samples was determined by one-way ANOVA for sorption and two-way ANOVA for desorption, followed by Dunnett's multiple comparisons test with a 5% significance level. The calculations were performed using GraphPad Prism v10 (GraphPad Software, LLC, San Diego, CA, USA).

For *in vitro* cytotoxicity studies, statistically significant differences between the cytotoxicity of BP/RSD and BP/RSD with a carrier were evaluated using one-way ANOVA followed by Tukey's *post hoc* test by GraphPad Prism 7.0 Software. Each sample was analysed in three separate experiments, with 5 wells per tested concentration (n = 15).

3. Results and discussion

The compounds selected for this work had previously been tested for their affinity to hydroxyapatite (the main bone-building material). All twelve aminomethylenebisphosphonates showed equal or stronger affinity for hydroxyapatite compared to the RSD.[12,33] This high affinity to hydroxyapatite highlights their potential as future drugs for osteoporosis treatment, making them suitable candidates for this study.

The sorption capacity of zeolite differed depending on which BPs were sorbed (Fig. 1). Analyzing the sorption results for the first week, we can distinguish two groups of compounds: those that sorbed strongly (above 80%), *i.e.* BP5, BP6, BP12, and RSD, and those that sorbed weakly (below 50%). In this group, we can also find compounds that underwent minimal sorption, *i.e.* BP1, BP7 and BP8 (sorption below 10%). During the first week of the sorption process, the concentration of BPs was monitored. Initially, some solutions showed lower concentrations, indicating higher sorption. However, the concentration gradually increased daily, resulting in a high BP concentration after one week, reflecting lower overall sorption. In none of the analyzed samples did the concentration exceed 50%. For further studies on release, only compounds that adsorbed more than 50% on the calcium zeolite were selected. The results of sorption are presented in Fig. 1.

BPs from the first group underwent additional sorption with subsequent doses of compound. BP12 maintained a consistent sorption level in the following two weeks compared to the first week, while BP5 exhibited a sorption level comparable to RSD only during the first week. The remaining compounds exhibited lower sorption rates. However, after three cycles, all four BPs were sorbed at over 50%. BP12 has a benziothiazole group instead of a pyridine ring, leading to a beneficial effect as its

Table 2 Absorption properties of the tested compounds

Compound	λ_{max}	ε_{max}	λ_{max}	ε_{max}
RSD	262	3143		
BP1	244	11 646	315.5	4320
BP2	243	10 480	311	5817
BP3	246	9166	310.5	4331
BP4	246	13 611	323	5371
BP5	246	9097	315.5	6046
BP6	254	14 526	325.5	1257
BP7	256	15 623	323.5	2594
BP8	254	17 954	323.5	2949
BP9	251	13 634	314	4297
BP10	256	12 857	317	2914
BP11	241.5	16 229	344	5566
BP12	224	21 680	280	11 463

sorption onto the zeolite carrier was achieved at a higher level compared to RSD. BP5 and BP6, containing iodine and two methyl groups, respectively, within the pyridine ring, exhibited a high level of sorption for these compounds. The compounds that were sorbed to the lowest extent contained bromine and chlorine in their structure.

The sorption of twelve BPs (BP1 to BP12) and RSD on calcium zeolite was evaluated using a one-way ANOVA. The results demonstrated significant differences among the tested compounds, confirming that the type of BP significantly influenced the sorption percentage. During the first week, statistical analysis revealed a highly significant effect of compound type on sorption values ($F_{12,42} = 1559$, $p < 0.0001$). In the second and third weeks, when only the four most strongly sorbed compounds were analyzed, the differences remained significant, though less pronounced ($F_{3,16} = 44.27$, $p < 0.0001$ for the second week and $F_{3,16} = 18.98$, $p < 0.0001$ for the third week). When the total sorption over three weeks was considered, statistical differences among compounds were also confirmed ($F_{3,16} = 26.21$, $p < 0.0001$). *Post hoc* analyses using Dunnett's multiple comparisons test ($\alpha = 0.05$) indicated significant differences for the main compound effect. Most BPs exhibited significantly different sorption profiles compared to the standard compound RSD. However, BP5 showed no significant difference from RSD only in the first week, while BP6 and BP12 sorbed at comparably high levels throughout the study, with BP12 consistently maintaining the same sorption level in each week.

The results of sorption were further validated using EDS, which characterized the zeolite both before and after drug sorption. The purpose of the measurement was to determine whether phosphorus ions, which indicate the presence of drugs, were present in the tested samples. Only samples BP5, BP6, BP12 and RSD showed significant amounts of phosphorus (Table 3) which confirmed the presence of phosphorus in the samples, indicating successful drug retention by the zeolite carrier. There is more of it on the surfaces of RSD and BP12 than on the surfaces of BP5 and BP6. Importantly, for the BP12 sample, the repeatability of the results is very low. It can be assumed that the drug is not evenly distributed throughout the zeolite carrier. The higher phosphorus content detected by EDS for RSD and BP12 compared to BP5 and BP6, despite similar

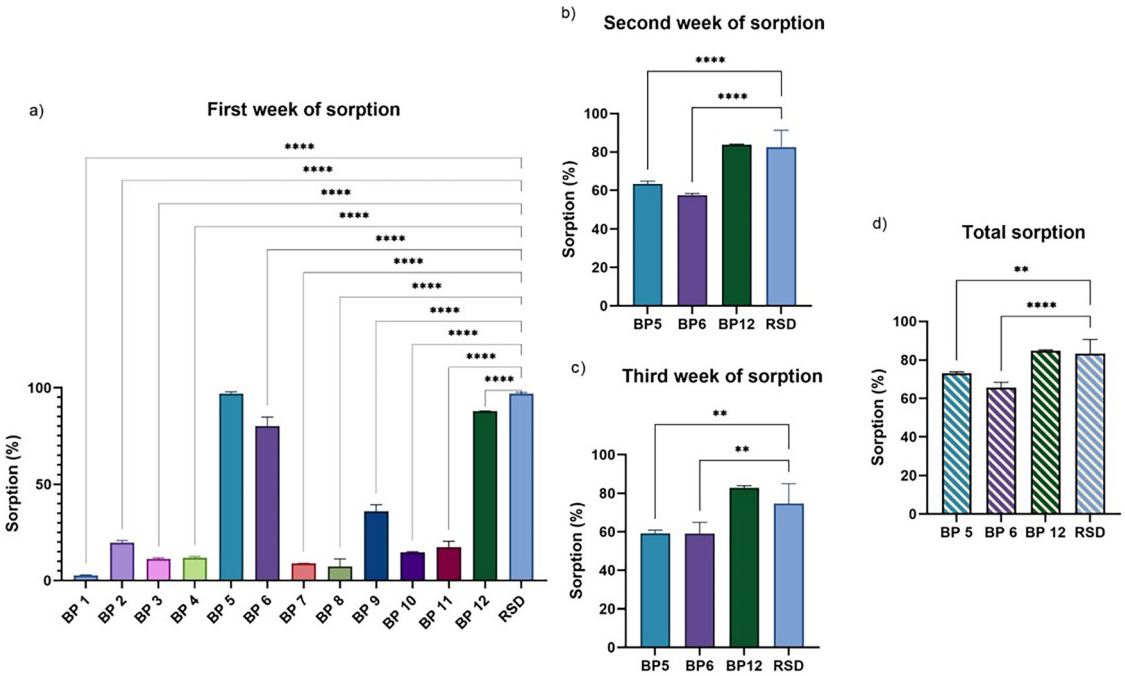

Fig. 1 Sorption of bisphosphonates (BPs) on the zeolite carrier over time. Sorption experiments were conducted over consecutive weeks. In the first week (a), all BPs (BP1–BP12) and risedronate (RSD) were tested. Only four compounds (BP5, BP6, BP12, and RSD) exhibited sorption above 50%. Consequently, only these four compounds were further analyzed in the second (b) and third (c) weeks by adding another portion of BPs to the system. In panel (d), the total sorption over three weeks was calculated by summing the values from all measurement points. Data are presented as mean ± SE ($N = 5$). A one-way ANOVA was conducted to examine differences in sorption values, followed by Dunnett's multiple comparisons test ($\alpha = 0.05$). Statistically significant differences are indicated as follows: *$p < 0.05$, **$p < 0.01$, ***$p < 0.001$, ****$p < 0.0001$.

Table 3 Phosphorus content in the tested materials determined on the basis of EDS results

Compound	Phosphorus content [at%]
CaX	0
RSD	3.36 ± 0.59
BP1	0
BP2	0
BP3	0
BP4	0
BP5	0.85 ± 0.45
BP6	0.20 ± 0.09
BP7	0
BP8	0
BP9	0
BP10	0
BP11	0
BP12	3.49 ± 6.59

sorption efficiencies, may result from differences in surface coverage or layer thickness. While RSD and BP12 likely form more compact or homogeneous layers on the zeolite surface, BP5 and BP6 may create thinner or more dispersed layers, leading to a weaker phosphorus signal in EDS analysis.

SEM images were also taken for the materials that retained the drug and are presented in Fig. 2 and ESI,† Fig. S1–S4. All materials show structures characteristic of zeolite. In the case of the BP12 material, additional structures can be noticed. These are elongated, hexagonal crystals that indicate that the drug is not only retained on the carrier but also creates metal–organic structures.[52] The hexagonal morphology rules out the possibility that these are larger zeolite particles, as the zeolite framework is cubic and does not crystallize in a hexagonal form. This explains the lack of reproducibility of the results in EDS analysis and may have a significant impact on the drug release profile.

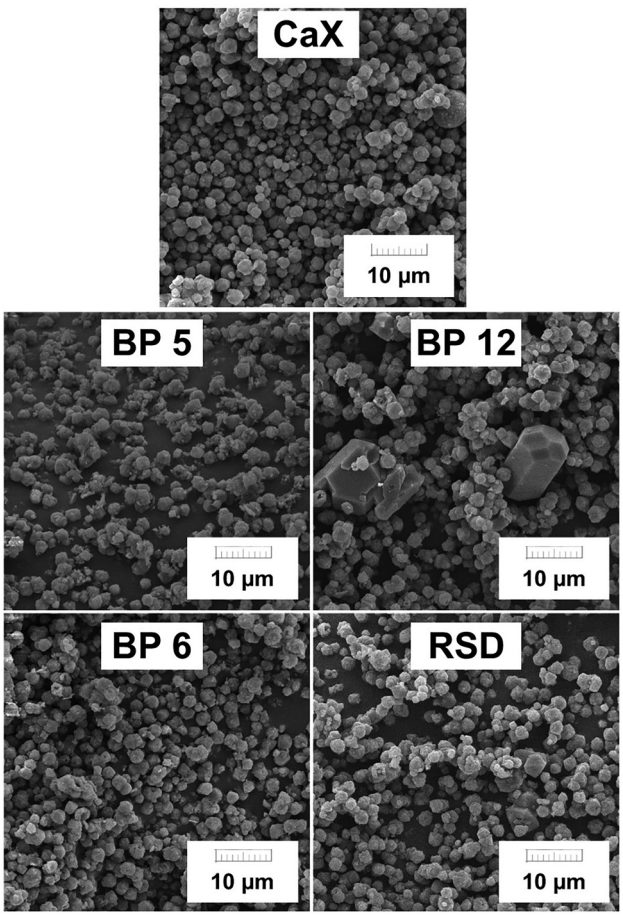

Fig. 2 SEM photos of the tested materials.

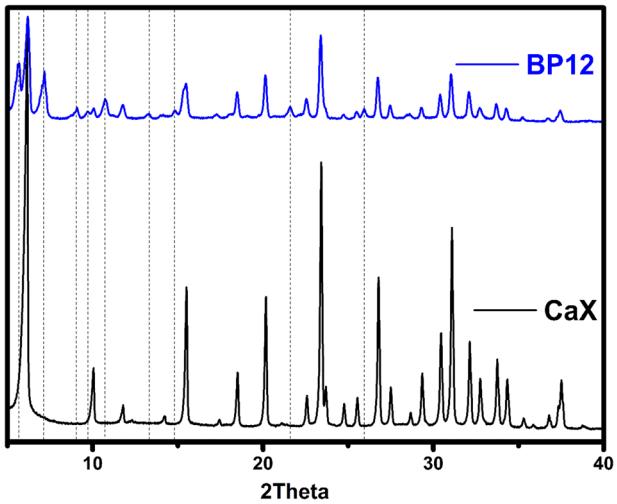

Fig. 3 X-ray diffraction (XRD) patterns of calcium-exchanged zeolite (CaX, black) and CaX after BP12 loading (blue).

The formation of new crystalline structures was also confirmed using X-ray diffraction (XRD) (Fig. 3). A comparison of the material before drug sorption (CaX) and after sorption (BP12) clearly indicates the formation of additional crystalline phases (Fig. 4). In the case of BP12, several additional diffraction peaks are visible, clearly suggesting that the drug is not only present on the surface of the zeolite but also exists as a separate, crystallized structure. These results are consistent with the SEM analysis and indicate the presence of an additional crystalline phase for this compound.

Another technique used to characterize the material was elemental analysis (Table 4). On this basis, it was also possible to confirm that the most drug was retained by BP12, and the least by BP6, and these results are consistent with the UV and EDS analysis.

The DFT calculations considered two BPs that are strongly adsorbed in the zeolite (BP5 and BP6) and two others for which adsorption is negligible (BP3 and BP7). We note that pairs of BPs are structurally similar: BP5 differs from BP3 by one additional methyl group and BP6 and BP7 differ only in the halogen substituent (BP6: iodine; BP7: bromine). The averaged adsorption energies are tabulated in Table 5, together with the relative contribution of dispersion interactions. Even though the $\Delta\bar{E}_{ads}$ values computed for the strongly adsorbed BPs are somewhat more negative than for the non-adsorbed ones, it is more noteworthy that all adsorption energies fall in a relatively narrow interval of about 30 kJ mol^{-1}, varying from −366 for

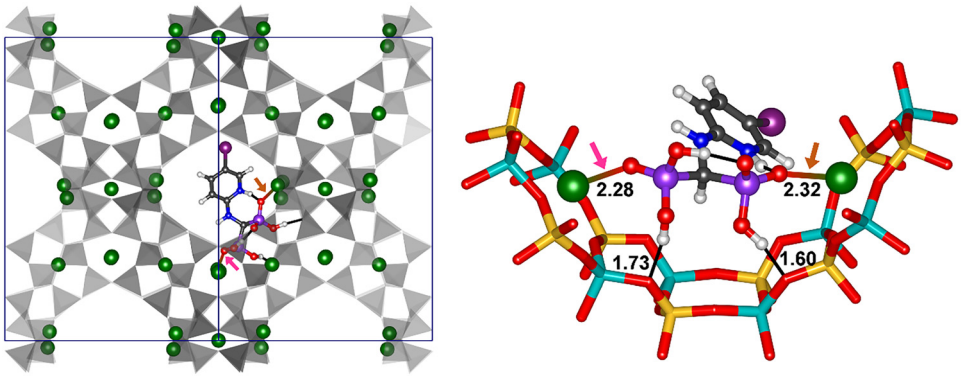

Fig. 4 Left: DFT-optimized lowest-energy configuration of BP6 in CaX. For clarity, the zeolite framework is displayed using grey tetrahedra, Ca^{2+} cations are shown as green spheres. Ca···O bonds are highlighted with arrows, hydrogen bonds are shown as light black lines. Projection along [110]. Right: Zoomed-in view of the local environment of BP6, emphasizing close contacts to framework atoms. The Ca···O and hydrogen bond distances are given in Å.

Table 4 Elemental analysis of carriers before and after drug sorption [wt%]

Compound	N%	C%
CaX	0	0.04 ± 0.01
RSD	3.46 ± 0.54	12.71 ± 1.63
BP5	3.86 ± 0.20	11.91 ± 1.18
BP6	3.54 ± 0.05	11.40 ± 0.10
BP12	4.78 ± 0.04	13.99 ± 0.11

BP3 to −398 kJ mol^{-1} for BP6. In particular, the adsorption energies of BP5 and BP7 fall very closely together, despite their qualitatively different adsorption behaviour. Thus, it has to be concluded that the observed, intricate differences in adsorption energy should not be overinterpreted, especially when considering the simplifications that are being made in the DFT calculations (for example, the neglect of water co-adsorption). We can primarily infer from these calculations that the strength of the host–guest interactions that is reflected in the adsorption energy does not, on its own, determine which BPs are adsorbed by the zeolite. It seems more likely that the experimentally observed differences in the adsorption behaviour of different BPs are the result of a complex interplay of factors that may include diffusion limitations, surface effects, and pore blockage by competitive water adsorption.

Dispersion interactions play an important role in stabilising the adsorbed BP molecules in the zeolite pores, with the relative contribution of dispersion interactions to the total adsorption energy varying from 0.45 to 0.55. Interestingly, this contribution is reduced for those two species that are strongly adsorbed by CaX, BP5 and BP6. This is a rather surprising observation, as the presence of the additional methyl group on BP5 and of the heavier iodine substituent on BP6 should generally tend to increase the contribution of dispersion in comparison to BP3 and BP7, respectively. In order to understand contributing factors beyond dispersion for a representative case, the lowest-energy configuration of BP6 adsorbed in CaX was visualized and analyzed in more detail. As is visible in the left panel of Fig. 4, the two phosphonic acid groups of the BP6 molecule interact with two Ca^{2+} cations on one side of the supercage (highlighted by arrows). The remaining part of the molecule protrudes across the supercage. The distances between the Ca^{2+} cations and the nearest BP6 oxygen atoms are on the order of 2.3 Å, somewhat shorter than the sum of ionic radii of 2.35 Å,[53] and thus indicative of a strong electrostatic interaction (Fig. 4, right panel). Besides, there are two fairly short hydrogen bonds from OH groups of BP6 to framework oxygen atoms (black lines in Fig. 4). Although the lowest-energy configurations of BP3, BP5, and BP7 adsorbed in CaX differ in some respects, they all include two short Ca···O bonds (on the order of 2.3 Å) and at least two hydrogen bonds to framework oxygen atoms. This shows that, besides ubiquitous dispersion interactions, strong electrostatic interactions with the Ca^{2+} cations and hydrogen bonds contribute to the stabilization of the BP molecules in the zeolite pores.

Table 5 DFT results: Boltzmann-weighted adsorption energies and relative contribution of dispersion interactions (ΔE_{ads}) to the adsorption energy of the lowest-energy configuration

	$\Delta\bar{E}_{ads}$ [kJ mol^{-1}]	$\Delta E_{disp}/\Delta E_{ads}$
BP3	−366	0.53
BP5	−389	0.48
BP6	−398	0.45
BP7	−385	0.55

While sorption provides crucial information about the drug's interaction with the carrier, investigating desorption is equally important for evaluating the release profile, which is key to the material's potential for controlled drug delivery. The cumulative release of RSD and three BPs (BP5, BP6, BP12) from a calcium zeolite carrier in SBF is presented in Fig. 5. A two-way ANOVA was conducted to examine the effects of BP type and time on the cumulative release values. The results showed significant main effects for both the compound type (F_{3507} = 2857, $p < 0.001$), and the time period ($F_{39\,507}$ = 134.3, $p < 0.001$), as well as significant interaction effects ($F_{117\,507}$ = 17.60, $p < 0.001$). Dunnett's multiple comparisons test with a significance level of 0.05 indicated significant differences for the main compound effect. The test showed that there were significant differences between RSD and BP6 ($p < 0.001$) and between RSD and BP12 ($p < 0.001$), but there was no significant difference between RSD and BP5 ($p = 0.972$).

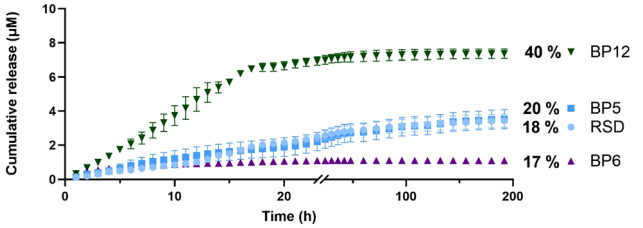

Fig. 5 Desorption of the BPs from the calcium zeolite carrier. The value presented as a percentage represents the percentage of the released compound calculated relative to the adsorbed amount. BP12 showed the highest cumulative release (~40%), characterized by a burst release phase in the first 12 h, likely due to surface crystallite desorption. In contrast, BP5 and RSD exhibited more gradual release profiles (~20% and ~18%, respectively), while BP6 displayed minimal release (~17%) and plateaued early. Data are presented as mean ± SD (N = 5), with the dotted lines representing the standard error of the mean. A two-way ANOVA was conducted to examine the effects of BP type and time on the cumulative release values. Dunnett's multiple comparisons test with a significance level of 0.05 indicated significant differences for the main compound. Detailed statistical analysis and *post hoc* comparisons are provided in the text.

Table 6 R^2 values for pseudo-first-order, Higuchi, and Korsmeyer–Peppas models fitted to the release profiles of bisphosphonates

Compound	Pseudo-first-order (R^2)	Higuchi model (R^2)	Korsmeyer–Peppas (R^2)
RSD	0.9355	0.7255	0.8082
BP5	0.8184	0.6693	0.7647
BP6	0.9272	—[a]	0.65
BP12	0.9634	0.257	0.6782

[a] The Higuchi model did not fit the BP6 data (R^2 negative), and is therefore omitted.

The analysis revealed significant main effects for both BP type and time, as well as a significant interaction effect. The obtained results indicate that the type of BP has a significant impact on the cumulative release. The BP12 release profile suggests a less sustained release, with a more pronounced initial release followed by a tapering off. This could lead to a rapid achievement of therapeutic levels but might require more frequent dosing or result in less prolonged efficacy. This release profile results from the fact that there are two types of structures in the BP12 material. The first is the organometallic structure, which can be seen in SEM photos, and the second is the carrier-ion-drug system. The presence of elongated hexagonal crystals observed in SEM images of the BP12-loaded material suggests the formation of secondary drug aggregates or organometallic crystalline phases outside the zeolite framework. This structural phenomenon is likely responsible for the burst release observed in the initial phase of the release profile, as these crystalline domains may desorb more readily or dissolve faster than molecules adsorbed within the zeolite pores. This hypothesis was further supported by XRD analysis, which revealed additional diffraction peaks in the BP12-loaded sample. The release profile of the remaining three BPs suggests a sustained release mechanism, with a gradual increase over the duration of the experiment. This can be beneficial for maintaining therapeutic levels over an extended period. Similar to risedronate, BP5's moderate release is also suitable for sustained release applications. With the lowest release rate, BP6 may be beneficial where even slower and more prolonged drug release is required. The slower release of BP6 as compared to BP5 goes hand in hand with a (somewhat) more negative DFT adsorption energy (Table 5). This indicates that the stronger interaction of BP6 with the zeolites slows down guest molecule diffusion, thereby reducing the release rate. Tuning the strength of host–guest interactions, for example, through cation exchange may therefore enable a modulation of the release behavior. Moreover, since only a fraction of the adsorbed BPs was released during the experimental period, the system shows promise for extended or sustained delivery beyond the time frame of this study.

The kinetic profiles indicate that release behavior is structure-dependent (Table 6). Among the tested compounds, BP12 exhibited a strong fit to the pseudo-first-order model (R^2 = 0.96), which is consistent with its faster and less controlled release, possibly due to partial crystallization. In contrast, BPs such as BP5 and RSD showed Fickian diffusion behavior ($n <$ 0.45 in the Korsmeyer–Peppas model), suggesting controlled release from within the zeolite structure.[54] These differences underline the role of molecular structure in determining drug–carrier interactions.

In our previous study,[33] experiments were conducted involving the exposure of *L. paracasei* to different BPs, revealing a notable impact on the assessed parameters. The obtained results indicate that a close correlation exists between alterations in cell membrane permeability and cell surface hydrophobicity, both of which are intricately linked to the toxicity levels of the compounds under scrutiny. Cell growth was significantly inhibited in the presence of BP9 and BP12. This indicates that these compounds have the strongest negative effect on the bacterial cells. The rest of the BPs, especially BP1 and BP5, can be considered as relatively mild compounds that do not disturb the beneficial bacterial cells. These findings suggest that the reduced cytotoxicity of BP5 and BP6 after zeolite immobilization may support their safety in clinical applications involving prolonged exposure, such as implant coatings. In contrast, the retained activity of BP12, even when loaded on the carrier, could be beneficial in settings where localized antimicrobial or anti-inflammatory action is desirable. The distinct release profiles and selective cytotoxic effects highlight the potential to tailor bisphosphonate–zeolite systems for different therapeutic contexts.

The next stage of the research was to determine the influence of the carrier on the biological properties of active substances – BPs. None of the tested drugs in a concentration range from 10–100 μM were significantly cytotoxic for fibroblasts *in vitro* (viability >50%) (Fig. 6(a), (c), (e) and (g)). The addition of a carrier has a significant influence on the properties of all active substances. For all substances it can be seen that the addition of a carrier reduces their cytotoxic properties towards fibroblasts (Fig. 6(a), (c), (e) and (g)). It is important that the carrier influences the reduction of drug cytotoxicity to health cells, so this should be considered a great advantage.

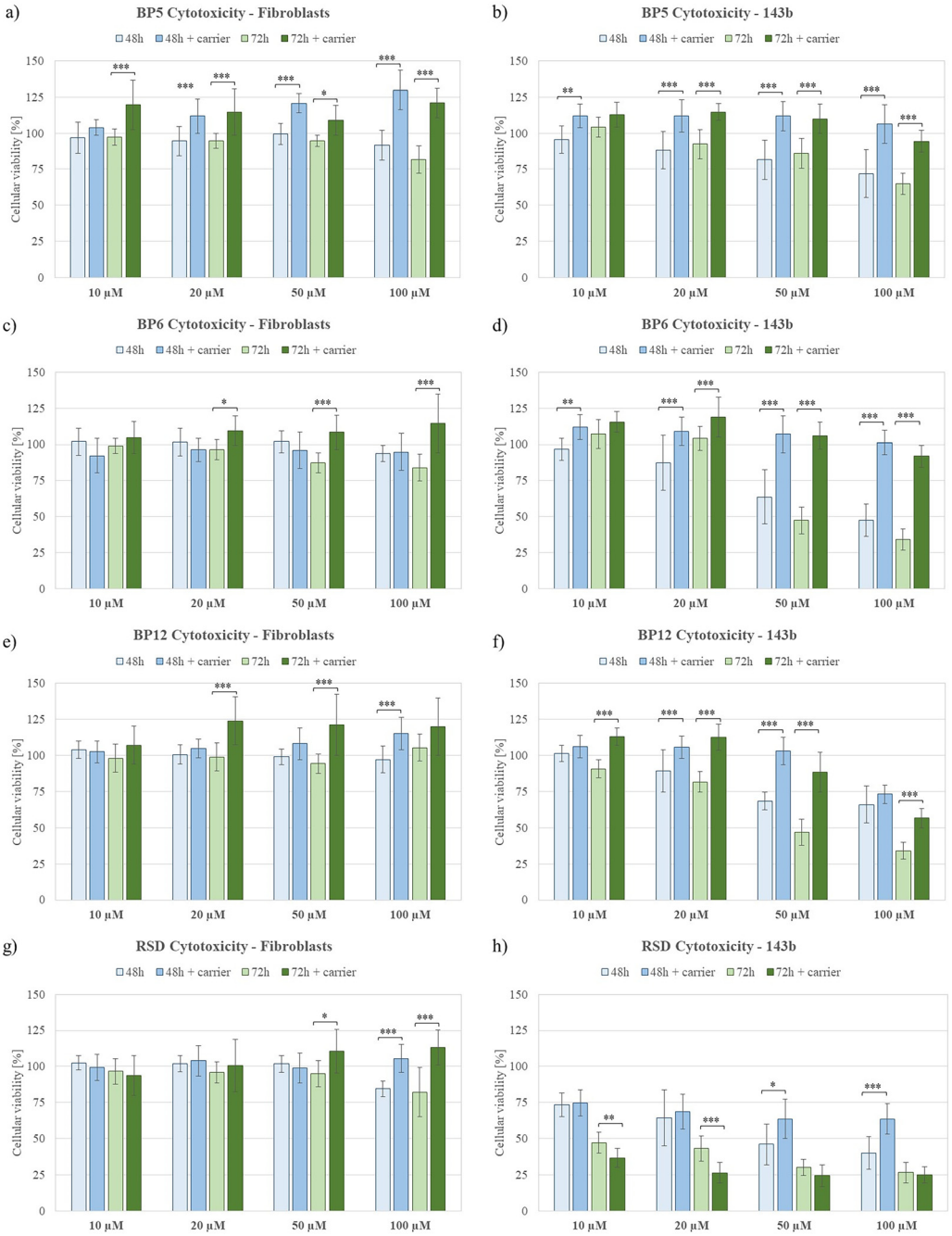

Fig. 6 Comparison of the *in vitro* cytotoxicity of free BPs and BPs with zeolite carriers against human fibroblasts and 143b osteosarcoma cells. Panels (a, c, e, g) show results for fibroblasts, and (b, d, f, h) for 143b cells, for BP5, BP6, BP12 and RSD, respectively. Bars represent mean viability ± SD of cells treated for 48 h or 72 h with 10–100 µM of the indicated compound. ***$p < 0.001$; **$p < 0.01$; *$p < 0.05$.

Many studies show that BPs exhibit antitumor activity. This is because they have the ability to inhibit key enzymatic pathways, such as the mevalonate pathway. This pathway is suppressed due to the ability of the BPs to inhibit farnesyl pyrophosphate synthase. Additionally, the BPs possess antiangiogenic properties, which hinder tumor development. Moreover, as mentioned in the introduction, BPs are used in cancer therapies as agents preventing bone metastases. Therefore, their ability to kill cancer cells remains crucial for effective therapy.[55–57]

As can be seen RSD showed significant cytotoxicity to the osteosarcoma 143b cell line at all tested concentrations, especially following 72 h treatment (cellular viability <50%) (Fig. 6(g)). The cytotoxicity of RSD towards osteosarcoma cells is consistent with previous literature reports.[58,59] Additionally, in the case of risedronate loaded onto a carrier, increased cytotoxicity against 143b cells can be observed after 72 hours of cell culture compared to risedronate without a carrier, particularly at lower concentrations of 10 µM and 20 µM

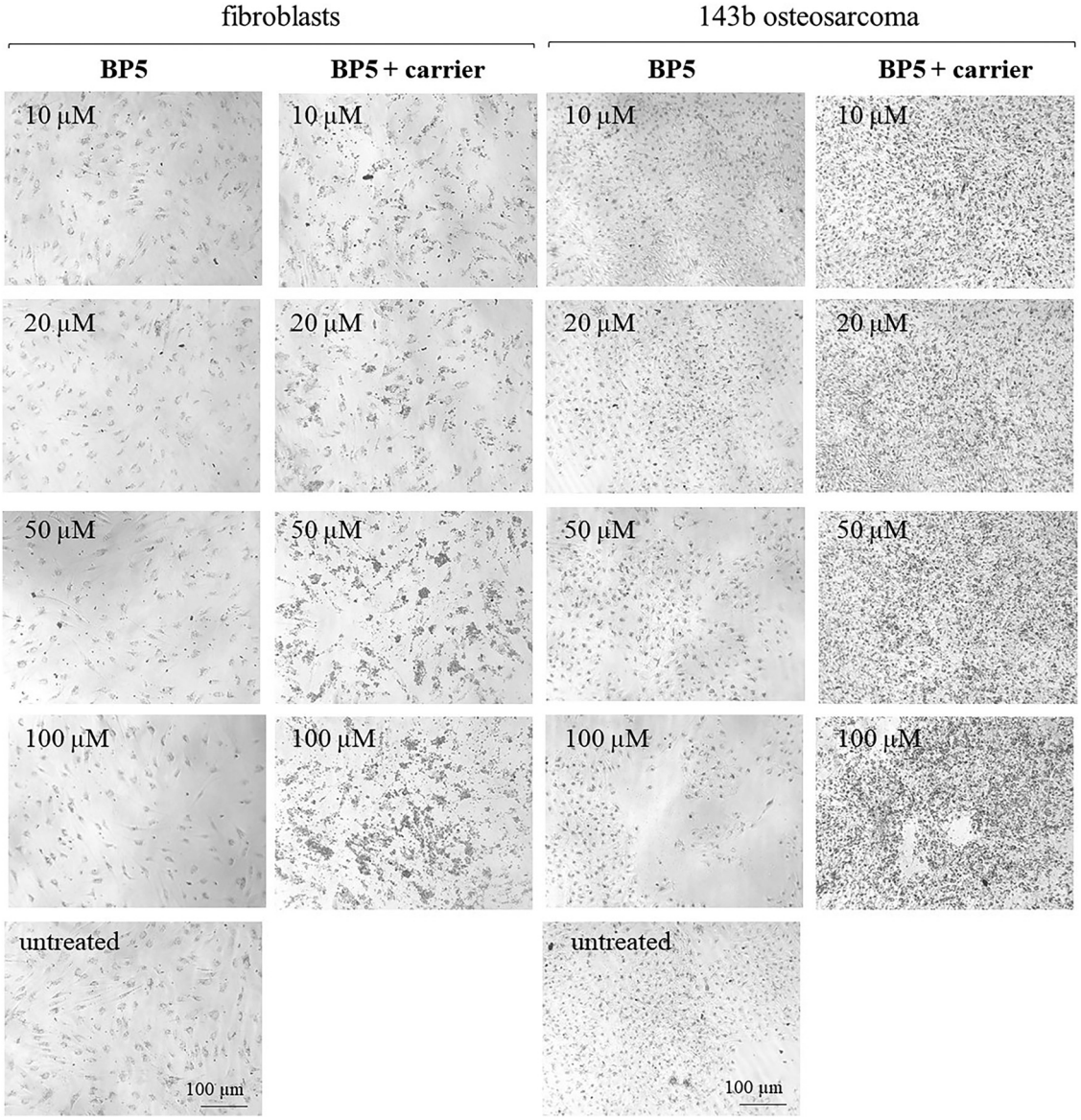

Fig. 7 Comparison of fibroblast and 143b osteosarcoma cell morphology, treated with free BP5 and BP5 with zeolite carrier for 72 h. Neutral red staining; pictures are representative for three experiments; magnification 40×, scale bar = 100 μm.

(Fig. 6(g)). BP6 and BP12 were also significantly cytotoxic, especially following 72 h exposure to the drugs at 50 μM and 100 μM (Fig. 6(d) and (f)). The cytotoxic effect of BP5 was less pronounced (Fig. 6(b)).

Adding the zeolite carrier to BP5 and BP6 eliminated the drug's cytotoxic effects on osteosarcoma 143b cells at all tested concentrations (Fig. 6(b) and (d)). For BP6 this can be related to the very small amount of BPs released during the analysis. For BP5 this is most likely related to the lower cytotoxicity of the compound itself. In respect of BP12 the addition of the zeolite carrier also decreased the cytotoxicity of the drug but the toxic effect at 100 μM was still significant, reducing the percentage of viable cells to *ca.* 50% (Fig. 6(f)). This observation aligns with the release data, which showed the highest initial release from this material. Based on the obtained results, it can be concluded that the material with the highest potential is CaX loaded with RSD. This is because, in the presence of the carrier, it demonstrated high biocompatibility with healthy cells and significant cytotoxicity against osteosarcoma cells, even at low concentrations (10 μM and 20 μM). The second material with high potential is the material loaded with BP12. Unfortunately, BP5 and BP6 lose their ability to kill osteosarcoma cells in the presence of the carrier, which makes their practical application impossible. The remaining obtained materials, in addition to their application as drug carriers for osteoporosis treatment, can be used for the preparation of scaffolds with anti-cancer properties, as well as personalized zeolite-coated titanium implants that prevent cancer recurrence after bone resection.

Analysis of cell morphology after treatment with the tested compounds for 48 hours (ESI,† Fig. S5–S8) and 72 hours (Fig. 7–10)

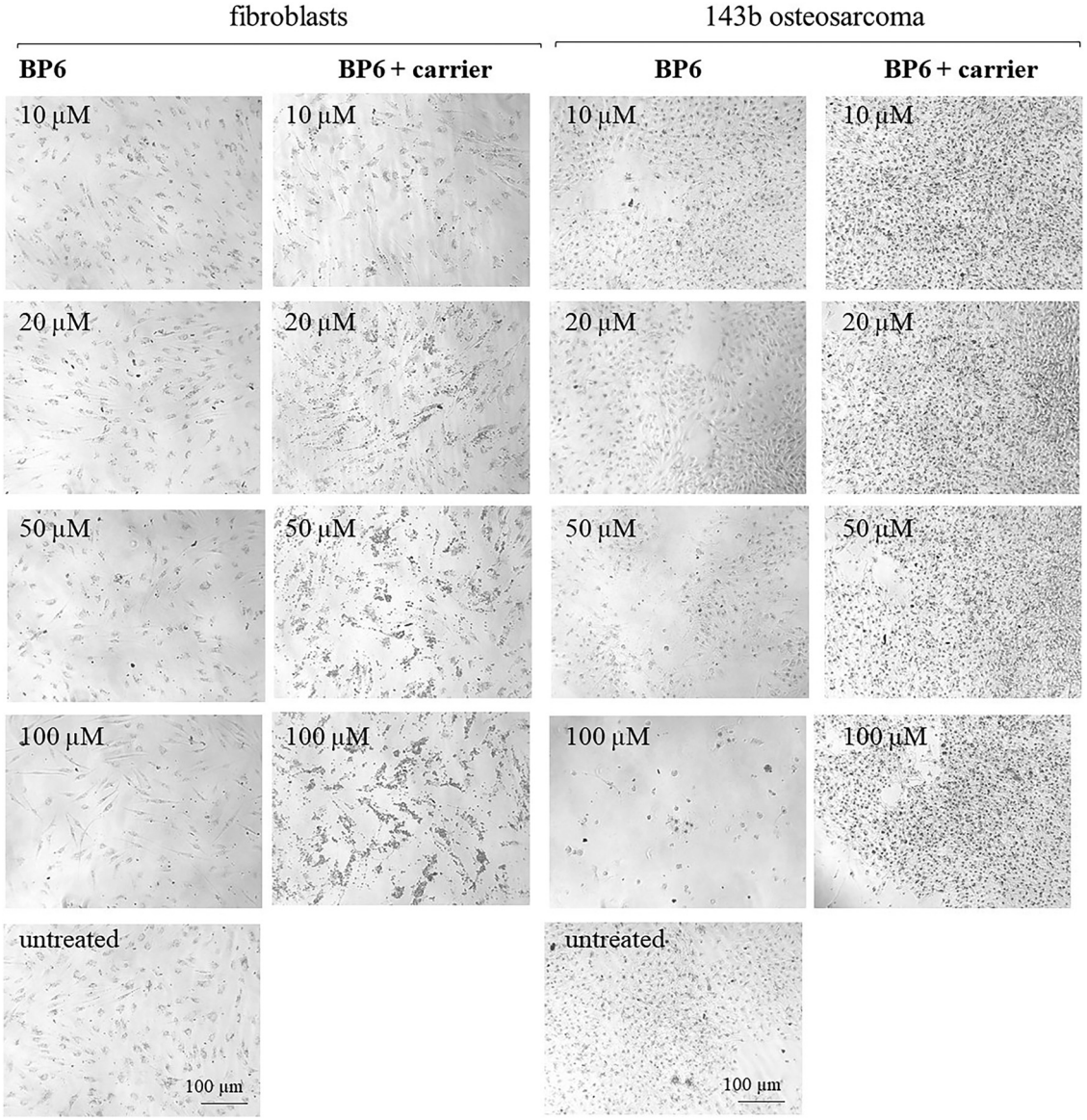

Fig. 8 Comparison of fibroblast and 143b osteosarcoma cell morphology, treated with free BP6 and BP6 with zeolite carrier for 72 h. Neutral red staining; pictures are representative for three experiments; magnification 40×, scale bar = 100 μm.

confirmed the results of the cytotoxicity assay. The combination of BP5 and BP6 with zeolites resulted in the loss of their anti-cancer potential (Fig. 7, 8 and Fig. S5, S6, ESI†). In the case of BP12 (Fig. 9 and Fig. S7, ESI†), the combination of the drug with a zeolite carrier reduced its anti-cancer activity but at 100 μM a significant reduction in viable cells was still noticeable. Combination of RSD with the zeolite carrier did not affect its anti-cancer effect but significantly increased the number of viable fibroblasts (Fig. 10 and Fig. S8, ESI†).

4. Conclusions

This study provides new insights into the sorption and release behavior of aminomethylenebisphosphonates using a calcium-exchanged zeolite carrier. In contrast to earlier work[23] focusing solely on commercial drugs, we evaluated a set of structurally novel BPs, using RSD as a reference. The extended sorption protocol (three weekly cycles) ensured high reproducibility and system equilibration. Our findings reveal that subtle structural variations between compounds can result in distinct binding interactions and release kinetics. This comparative structure–function analysis, supported by kinetic modeling, highlights the importance of molecular design in optimizing drug–carrier systems and represents a significant step forward in the development of targeted delivery platforms for bone-active compounds.

The zeolite carrier demonstrated a high sorption capacity for certain BPs, with BP5, BP6, BP12, and RSD showing sorption levels above 80% during the first week. This indicates strong interactions between these BPs and the zeolite carrier, facilitating effective drug loading. Different BPs exhibited distinct sorption and release profiles. BP12 showed the highest sorption

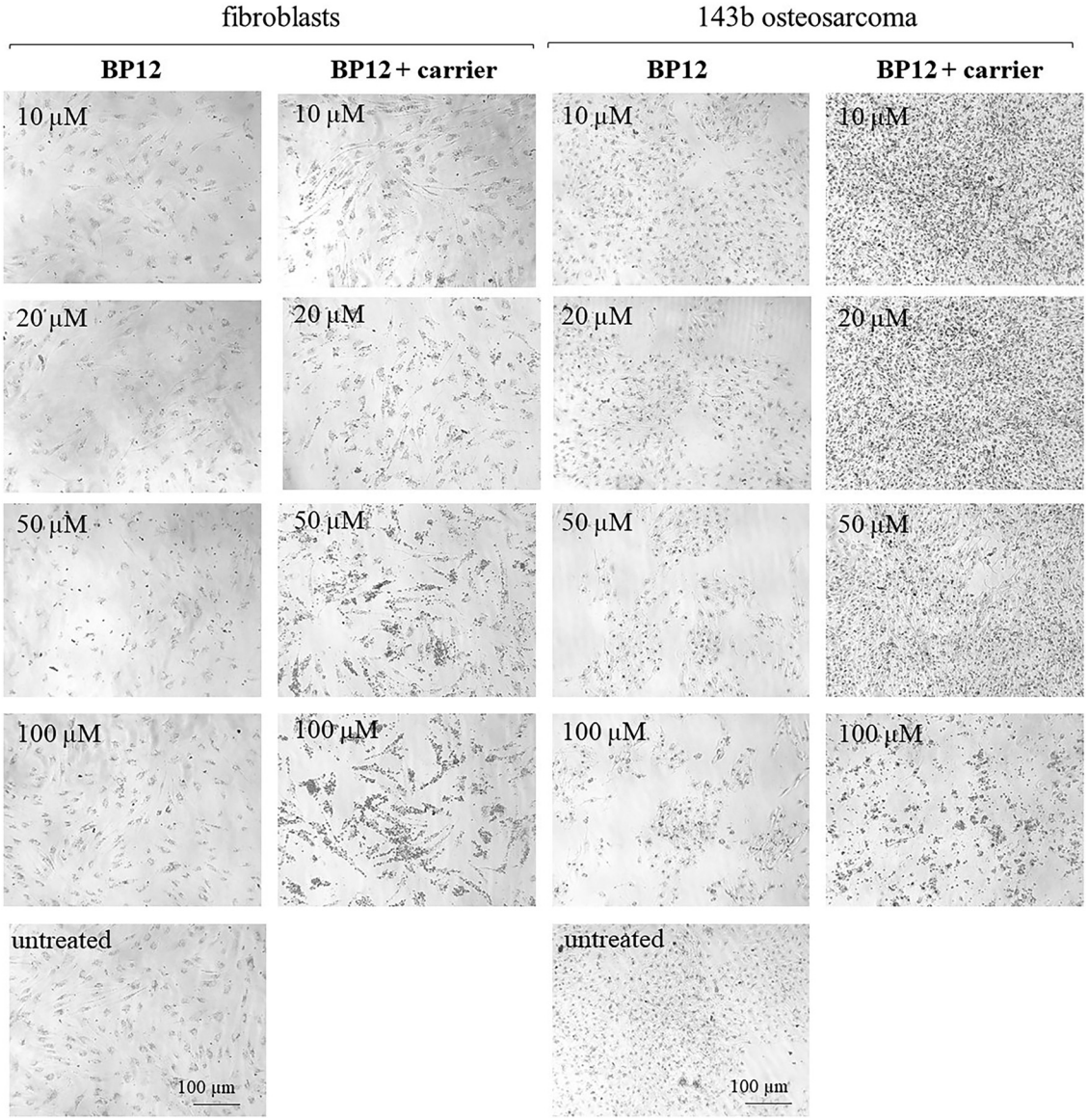

Fig. 9 Comparison of fibroblast and 143b osteosarcoma cell morphology, treated with free BP12 and BP12 with zeolite carrier for 72 h. Neutral red staining; pictures are representative for three experiments; magnification 40×, scale bar = 100 μm.

levels, likely due to the presence of a benziothiazole group, which enhanced its affinity for the zeolite carrier. SEM analysis revealed the presence of large crystalline structures in BP12, suggesting that, in addition to adsorption onto the carrier, the drug also forms separate crystalline deposits. This variability in drug distribution could account for the pronounced differences in phosphorus content detected *via* EDS and may significantly influence the release profile of BP12. The BPs containing iodine and methyl groups (BP5 and BP6) also exhibited high sorption, while those with bromine and chlorine showed lower sorption levels. The release profiles of risedronate, BP5, and BP6 indicated a sustained release mechanism, with gradual desorption over time. The sustained release of RSD and BP5 makes them suitable candidates for long-term management of conditions like osteoporosis, where maintaining steady drug levels is crucial. Controlled release is beneficial for maintaining therapeutic levels over extended periods, reducing the need for frequent dosing. The BP6, with the slowest release rate, may be advantageous in scenarios requiring extremely prolonged drug delivery. BP12, however, exhibited a more pronounced initial release followed by a tapering off, suggesting that it may be suitable for applications requiring a rapid therapeutic onset, but might necessitate more frequent dosing. Additionally, only a portion of the adsorbed BPs was released during the study period, indicating the potential for further prolonged drug release over an extended duration.

The computational modeling (DFT) provided insights into the adsorption mechanisms, highlighting the contributions of electrostatic interactions, hydrogen bonding, and dispersion forces in stabilizing the adsorbed molecules. The stronger

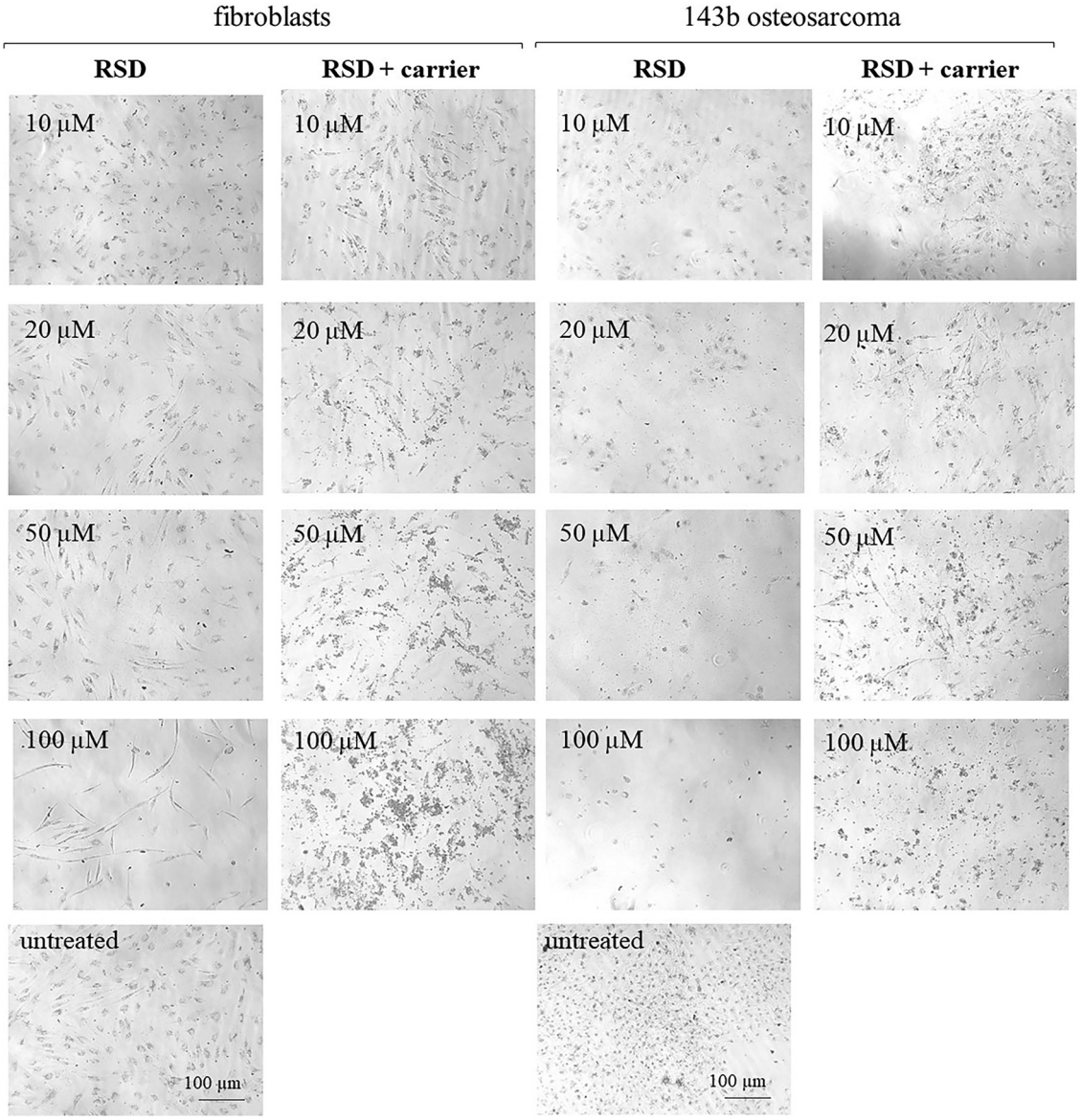

Fig. 10 Comparison of fibroblast and 143b osteosarcoma cell morphology, treated with free RSD and RSD with zeolite carrier for 72 h. Neutral red staining; pictures are representative for three experiments; magnification 40×, scale bar = 100 μm.

interaction with BP6 as compared to BP5 might be responsible for the slower release of BP6. Beyond this, the differences in adsorption energy were too subtle to fully explain the large differences in sorption behavior among several BPs. This suggests that other factors, such as diffusion limitations and surface effects, may also play significant roles. The addition of a zeolite carrier reduced the cytotoxicity towards fibroblasts, while RSD and BP12 retained strong activity against osteosarcoma 143b cells, making them promising candidates for targeted therapies. In contrast, BP5 and BP6 lost their cytotoxic effects in cancer cells, limiting their potential application.

In conclusion, the use of calcium-exchanged zeolite carriers for aminomethylenebisphosphonates offers promising potential for controlled and sustained drug release, with significant implications for the treatment of osteoporosis and other related conditions. Additionally, their selective cytotoxic effects open new possibilities for their application in cancer therapy, particularly in osteosarcoma treatment. Further research is warranted to explore the full scope of these carriers in diverse biomedical applications. It should be emphasized that the presented results are merely a proof of concept, and these studies require further continuation. The release profiles may be influenced by various factors such as a change in process scale, altered particle size, the formation of layers on implant surfaces, or incorporation as part of scaffolds. However, the results obtained so far are promising. The key aspects—namely controlled release and the reduction of cytotoxicity—confirmed in this study even after scaling up or applying the material in a specific context, should remain unchanged and clearly demonstrate the novelty and innovativeness of the presented materials.

Conflicts of interest

The authors declare that they have no known competing financial interests or personal relationships that could have appeared to influence the work reported in this paper.

Data availability

Data supporting the findings of this study are available in the open RepOD repository with the identifier 10.18150/UEEQCZ.

Acknowledgements

This paper was produced with financial support from the Polish National Science Centre (grant number UMO-2020/39/B/ST5/00320). Michael Fischer gratefully acknowledges funding by the Deutsche Forschungsgemeinschaft (German Research Foundation, DFG) through a Heisenberg fellowship (project no. 455871835), as well as computing time granted by the Resource Allocation Board and provided on the supercomputers Lise and Emmy at NHR@ZIB and NHR@Göttingen as part of the NHR infrastructure. The DFT calculations for this research were conducted with computing resources under the project hbc00062.

References

1 M.-F. Heymann, F. Lezot and D. Heymann, Bisphosphonates in common pediatric and adult bone sarcomas, *Bone*, 2020, **139**, 115523, DOI: 10.1016/j.bone.2020.115523.
2 P. Clézardin, F. H. Ebetino and P. G. J. Fournier, Bisphosphonates and Cancer-Induced Bone Disease: Beyond Their Antiresorptive Activity, *Cancer Res.*, 2005, **65**, 4971–4974, DOI: 10.1158/0008-5472.CAN-05-0264.
3 T. Ohba, J. M. M. Cates, H. A. Cole, D. A. Slosky, H. Haro and J. Ichikawa, *et al.*, Pleiotropic effects of bisphosphonates on osteosarcoma, *Bone*, 2014, **63**, 110–120, DOI: 10.1016/j.bone.2014.03.005.
4 N. Horie, H. Murata, Y. Nishigaki, T. Matsui, H. Segawa and M. Nogawa, *et al.*, The third-generation bisphosphonates inhibit proliferation of murine osteosarcoma cells with induction of apoptosis, *Cancer Lett.*, 2006, **238**, 111–118, DOI: 10.1016/j.canlet.2005.06.041.
5 T. Ohba, H. A. Cole, J. M. Cates, D. A. Slosky, H. Haro and T. Ando, *et al.*, Bisphosphonates Inhibit Osteosarcoma-Mediated Osteolysis Via Attenuation of Tumor Expression of MCP-1 and RANKL, *J. Bone Miner. Res.*, 2014, **29**, 1431–1445, DOI: 10.1002/jbmr.2182.
6 G. Clunie and R. W. Keen, *Osteoporosis*, Oxford University Press, Oxford, 2nd edn, 2014.
7 J. E. Compston, M. R. McClung and W. D. Leslie, Osteoporosis, *Lancet*, 2019, **393**, 364–376, DOI: 10.1016/S0140-6736(18)32112-3.
8 J. A. Kanis, N. Norton, N. C. Harvey, T. Jacobson, H. Johansson and M. Lorentzon, *et al.*, SCOPE 2021: a new scorecard for osteoporosis in Europe, *Arch. Osteoporos*, 2021, **16**, 82, DOI: 10.1007/s11657-020-00871-9.
9 C. Willers, N. Norton, N. C. Harvey, T. Jacobson, H. Johansson and M. Lorentzon, *et al.*, Osteoporosis in Europe: a compendium of country-specific reports, *Arch. Osteoporos.*, 2022, **17**, 23, DOI: 10.1007/s11657-021-00969-8.
10 L. Widler, K. A. Jaeggi, M. Glatt, K. Müller, R. Bachmann and M. Bisping, *et al.*, Highly Potent Geminal Bisphosphonates. From Pamidronate Disodium (Aredia) to Zoledronic Acid (Zometa), *J. Med. Chem.*, 2002, **45**, 3721–3738, DOI: 10.1021/jm020819i.
11 R. G. G. Russell, Z. Xia, J. E. Dunford, U. Oppermann, A. Kwaasi and P. A. Hulley, *et al.*, Bisphosphonates: An Update on Mechanisms of Action and How These Relate to Clinical Efficacy, *Ann. N. Y. Acad. Sci.*, 2007, **1117**, 209–257, DOI: 10.1196/annals.1402.089.
12 M. Zielińska, E. Chmielewska, T. Buchwald, A. Voelkel and P. Kafarski, Determination of bisphosphonates anti-resorptive properties based on three forms of ceramic materials: Sorption and release process evaluation, *J. Pharm. Anal.*, 2021, **11**, 364–373, DOI: 10.1016/j.jpha.2020.07.011.
13 R. G. G. Russell, Bisphosphonates: From Bench to Bedside, *Ann. N. Y. Acad. Sci.*, 2006, **1068**, 367–401, DOI: 10.1196/annals.1346.041.
14 R. Bartl, B. Frisch, E. Von Tresckow and C. Bartl, *Bisphosphonates in Medical Practice*, Springer, Berlin Heidelber, 2007, DOI: 10.1007/978-3-540-69870-8.
15 N. J. Bishop and G. Russell, Bisphosphonates, *Osteogenesis Imperfecta*, Elsevier, 2014, pp. 495–500, DOI: 10.1016/B978-0-12-397165-4.00053-8.
16 M. Zielińska, G. Garbacz, J. Sczodrok and A. Voelkel, The Effects of Various Food Products on Bisphosphonate's Availability, *Pharmaceutics*, 2022, **14**, 717, DOI: 10.3390/pharmaceutics14040717.
17 The National Osteoporosis Guideline Group (NOGG), J. Compston, A. Cooper, C. Cooper, N. Gittoes and C. Gregson, *et al.*, UK clinical guideline for the prevention and treatment of osteoporosis, *Arch. Osteoporos.*, 2017, **12**, 43, DOI: 10.1007/s11657-017-0324-5.
18 G. Ficarra and F. Beninati, Bisphosphonate – related osteonecrosis of the jaws: the point of view of the oral pathologist, *Clin. Cases Miner. Bone Metab.*, 2007, **4**(1), 53–57.
19 C. Heng, V. M. Badner and R. Johnson, Bisphosphonate-Related Osteonecrosis of the Jaw in Patients with Osteoporosis, *Am. Fam. Physician*, 2012, **85**(12), 1134–1141.
20 X. Zhang, I. S. Hamadeh, S. Song, J. Katz, J. S. Moreb and T. Y. Langaee, *et al.*, Osteonecrosis of the Jaw in the United States Food and Drug Administration's Adverse Event Reporting System (FAERS): DRUG INDUCED ONJ AND FAERS DATABASE, *J. Bone Miner. Res.*, 2016, **31**, 336–340, DOI: 10.1002/jbmr.2693.
21 M. Usman, Recent Progress of SAPO-34 Zeolite Membranes for CO2 Separation: A Review, *Membranes*, 2022, **12**, 507, DOI: 10.3390/membranes12050507.
22 A. Fabiano, A. M. Piras, V. Calderone, L. Testai, L. Flori and D. Puppi, *et al.*, A New Calcium Oral Controlled-Release System Based on Zeolite for Prevention of Osteoporosis, *Nutrients*, 2019, **11**, 2467, DOI: 10.3390/nu11102467.

23 M. Sandomierski, M. Zielińska and A. Voelkel, Calcium zeolites as intelligent carriers in controlled release of bisphosphonates, *Int. J. Pharm.*, 2020, **578**, 119117, DOI: 10.1016/j.ijpharm.2020.119117.

24 M. Vassaki, C. Kotoula, P. Turhanen, D. Choquesillo-Lazarte and K. D. Demadis, Calcium and Strontium Coordination Polymers as Controlled Delivery Systems of the Anti-Osteoporosis Drug Risedronate and the Augmenting Effect of Solubilizers, *Appl. Sci.*, 2021, **11**, 11383, DOI: 10.3390/app112311383.

25 P. Hissae Yassue-Cordeiro, C. H. Zandonai, B. Pereira Genesi, P. Santos Lopes, E. Sanchez-Lopez, M. L. Garcia, N. R. Camargo Fernandes-Machado, P. Severino, E. B. Souto and C. Ferreira da Silva, Development of Chitosan/Silver Sulfadiazine/Zeolite Composite Films for Wound Dressing, *Pharmaceutics*, 2019, **11**, 535, DOI: 10.3390/pharmaceutics11100535.

26 J. Liu, L. Yan, S. He and J. Hu, Engineering DNA quadruplexes in DNA nanostructures for biosensor construction, *Nano Res.*, 2022, **15**, 3504–3513, DOI: 10.1007/s12274-021-3869-y.

27 J. A. Park, C. Amri, Y. Kwon, J.-H. Lee and T. Lee, Recent Advances in DNA Nanotechnology for Plasmonic Biosensor Construction, *Biosensors*, 2022, **12**, 418, DOI: 10.3390/bios12060418.

28 Y. Li, Y. Cai, T. Chen and X. Bao, Zeolites: A series of promising biomaterials in bone tissue engineering, *Front. Bioeng. Biotechnol.*, 2022, **10**, 1066552, DOI: 10.3389/fbioe.2022.1066552.

29 M. Mousavi, A. E. Nejad, E. Shamsoddin, M. M. Golabgiran and B. Houshmand, Zeolite as a Bone Bio-Modifier Carrier: An *In Vitro* Study, *J. Microbiol. Biotechnol. Res.*, 2019, **9**, 126, DOI: 10.5539/jmbr.v9n1p126.

30 P. Zarrintaj, G. Mahmodi, S. Manouchehri, A. H. Mashhadzadeh, M. Khodadadi and M. Servatan, *et al.*, Zeolite in tissue engineering: Opportunities and challenges, *MedComm*, 2020, **1**, 5–34, DOI: 10.1002/mco2.5.

31 M. Sandomierski, M. Jakubowski, M. Ratajczak, M. Pokora, M. Zielińska and A. Voelkel, Release of drugs used in the treatment of osteoporosis from zeolites with divalent ions—Influence of the type of ion and drug on the release profile, *J. Biomed. Mater. Res.*, 2023, **111**, 1005–1014, DOI: 10.1002/jbm.b.35209.

32 M. Sandomierski, M. Jakubowski, M. Ratajczak, M. Pokora, M. Zielińska and A. Voelkel, Release of drugs used in the treatment of osteoporosis from zeolites with divalent ions-Influence of the type of ion and drug on the release profile, *J. Biomed. Mater. Res., Part B*, 2023, **111**, 1005–1014, DOI: 10.1002/jbm.b.35209.

33 M. Zielińska, A. Pacholak, N. Burlaga, E. Chmielewska, A. Voelkel and E. Kaczorek, Determination of bisphosphonate properties in terms of bioavailability, bone affinity, and cytotoxicity, *Pharmacol. Rep.*, 2024, **76**, 1160–1173, DOI: 10.1007/s43440-024-00624-2.

34 E. Matczak-Jon, K. Ślepokura and P. Kafarski, Solid state and solution behaviour of *N*-(2-pyridyl)- and *N*-(4-methyl-2-pyridyl)aminomethane-1,1-diphosphonic acids, *J. Mol. Struct.*, 2006, **782**, 81–93, DOI: 10.1016/j.molstruc.2005.07.004.

35 E. Matczak-Jon, W. Sawka-Dobrowolska, P. Kafarski and V. Videnova-Adrabińska, Molecular organization and solution properties of N-substituted aminomethane-1,1-diphosphonic acids, *New J. Chem.*, 2001, **25**, 1447–1457, DOI: 10.1039/b102282m.

36 S. Ghosh, J. M. W. Chan, C. R. Lea, G. A. Meints, J. C. Lewis and Z. S. Tovian, *et al.*, Effects of Bisphosphonates on the Growth of *Entamoeba histolytica* and *Plasmodium* Species *in Vitro* and *in Vivo*, *J. Med. Chem.*, 2004, **47**, 175–187, DOI: 10.1021/jm030084x.

37 E. Matczak-Jon, K. Slepokura and P. Kafarski, [(5-Bromopyridinium-2-ylamino)(phosphono)methyl]phosphonate, *Acta Crystallogr., Sect. C: Struct. Chem.*, 2006, **62**, 132–135.

38 E. Matczak-Jon and P. Kafarski, Conformations and resulting hydrogen-bonded networks of hydrogen {phosphono-[(pyridin-1-ium-3-yl)amino]methyl}phosphonate and related 2-chloro and 6-chloro derivatives, *Acta Crystallogr., Sect. C: S truct. Chem.*, 2011, **67**, o450–o456.

39 T. Kokubo and H. Takadama, How useful is SBF in predicting *in vivo* bone bioactivity?, *Biomaterials*, 2006, **27**, 2907–2915, DOI: 10.1016/j.biomaterials.2006.01.017.

40 M. Pietrzyńska and A. Voelkel, Stability of simulated body fluids such as blood plasma, artificial urine and artificial saliva, *Microchem. J.*, 2017, **134**, 197–201, DOI: 10.1016/j.microc.2017.06.004.

41 A. Domke, M. Fischer, M. Jakubowski, A. Pacholak, M. Ratajczak and A. Voelkel, *et al.*, Experimental and computational study on the Ca^{2+}, Mg^{2+}, Zn^{2+} and Sr^{2+} exchanged zeolites as a drug delivery system for fluoroquinolone antibiotic – Ciprofloxacin, *J. Drug Delivery Sci. Technol.*, 2024, **99**, 105997, DOI: 10.1016/j.jddst.2024.105997.

42 R. L. C. Akkermans, N. A. Spenley and S. H. Robertson, COMPASS III: automated fitting workflows and extension to ionic liquids, *Mol. Simul.*, 2021, **47**, 540–551, DOI: 10.1080/08927022.2020.1808215.

43 J. VandeVondele, M. Krack, F. Mohamed, M. Parrinello, T. Chassaing and J. Hutter, Quickstep: Fast and accurate density functional calculations using a mixed Gaussian and plane waves approach, *Comput. Phys. Commun.*, 2005, **167**, 103–128, DOI: 10.1016/j.cpc.2004.12.014.

44 T. D. Kühne, M. Iannuzzi, M. Del Ben, V. V. Rybkin, P. Seewald and F. Stein, *et al.*, CP2K: An electronic structure and molecular dynamics software package - Quickstep: Efficient and accurate electronic structure calculations, *J. Chem. Phys.*, 2020, **152**, 194103, DOI: 10.1063/5.0007045.

45 A. D. Becke, Density-Functional Thermochemistry. V. Systematic Optimization of Exchange-Correlation Functionals, *J. Chem. Phys.*, 1997, **107**, 8554–8560, DOI: 10.1063/1.475007.

46 S. Grimme, J. Antony, S. Ehrlich and H. Krieg, A consistent and accurate *ab initio* parametrization of density functional dispersion correction (DFT-D) for the 94 elements H-Pu, *J. Chem. Phys.*, 2010, **132**, 154104, DOI: 10.1063/1.3382344.

47 S. Grimme, Semiempirical GGA-Type Density Functional Constructed with a Long-Range Dispersion Correction, *J. Comput. Chem.*, 2006, **27**, 1787–1799, DOI: 10.1002/jcc.20495.

48 J. VandeVondele and J. Hutter, Gaussian basis sets for accurate calculations on molecular systems in gas and condensed phases, *J. Chem. Phys.*, 2007, **127**, 114105, DOI: **10.1063/1.2770708**.

49 M. Krack, Pseudopotentials for H to Kr optimized for gradient-corrected exchange-correlation functionals, *Theor. Chem. Acc.*, 2005, **114**, 145–152, DOI: **10.1007/s00214-005-0655-y**.

50 M. Fischer, Adsorption of Carbamazepine in All-Silica Zeolites Studied with Density Functional Theory Calculations, *ChemPhysChem*, 2023, **24**, e202300022, DOI: **10.1002/cphc.202300022**.

51 G. Repetto, A. del Peso and J. L. Zurita, Neutral red uptake assay for the estimation of cell viability/cytotoxicity, *Nat. Protoc.*, 2008, **3**, 1125–1131, DOI: **10.1038/nprot.2008.75**.

52 M. Vassaki, K. E. Papathanasiou, C. Hadjicharalambous, D. Chandrinou, P. Turhanen and D. Choquesillo-Lazarte, *et al.*, Self-sacrificial MOFs for ultra-long controlled release of bisphosphonate anti-osteoporotic drugs, *Chem. Commun.*, 2020, **56**, 5166–5169, DOI: **10.1039/D0CC00439A**.

53 R. D. Shannon, Revised Effective Ionic Radii and Systematic Studies of Interatomic Distances in Halides and Chalcogenides, *Acta Crystallogr., Sect. A*, 1976, **32**, 751–767, DOI: **10.1107/S0567739476001551**.

54 S. Dash, P. N. Murthy, L. Nath and P. Chowdhury, Kinetic Modeling On Drug Release From Controlled Drug Delivery Systems, *Acta Pol. Pharm.*, 2010, **67**(3), 217–223.

55 N. M. La-Beck, X. Liu, H. Shmeeda, C. Shudde and A. A. Gabizon, Repurposing amino-bisphosphonates by liposome formulation for a new role in cancer treatment, *Semin. Cancer Biol.*, 2021, **68**, 175–185, DOI: **10.1016/j.semcancer.2019.12.001**.

56 K. M. Au, A. Satterlee, Y. Min, X. Tian, Y. S. Kim and J. M. Caster, *et al.*, Folate-targeted pH-responsive calcium zoledronate nanoscale metal-organic frameworks: Turning a bone antiresorptive agent into an anticancer therapeutic, *Biomaterials*, 2016, **82**, 178–193, DOI: **10.1016/j.biomaterials.2015.12.018**.

57 J. Green and A. Lipton, Anticancer properties of zoledronic acid, *Cancer Invest.*, 2010, **28**, 944–957, DOI: **10.3109/07357907.2010.512598**.

58 T. Murayama, Y. Kawasoe, Y. Yamashita, Y. Ueno, S. Minami and M. Yokouchi, *et al.*, Efficacy of the Third-generation Bisphosphonate Risedronate Alone and in Combination with Anticancer Drugs Against Osteosarcoma Cell Lines, *Anticancer Res.*, 2008, **28**, 2147–2154.

59 Z. F. Xin, Y. K. Kim and S. T. Jung, Risedronate inhibits human osteosarcoma cell invasion, *J. Exp. Clin. Cancer Res.*, 2009, **28**, 105, DOI: **10.1186/1756-9966-28-105**.